Received May 7, 2021, accepted May 13, 2021, date of publication May 17, 2021, date of current version May 25, 2021.

Digital Object Identifier 10.1109/ACCESS.2021.3081068

Parametric Study of a Fully 3D-Printed Dielectric Resonator Antenna Loaded With a Metallic Cap

MATIAS CUEVAS, FRANCISCO PIZARRO, (Member, IEEE), ARIEL LEIVA, GABRIEL HERMOSILLA, AND DANIEL YUNGE, (Member, IEEE)

Escuela de Ingeniería Eléctrica, Pontificia Universidad Católica de Valparaíso, Valparaíso 2362804, Chile

Corresponding author: Francisco Pizarro (francisco.pizarro.t@pucv.cl)

This work was supported by the ANID INICIACION under Grant 11180434.

ABSTRACT This article presents a parametric study of a fully 3D-printed hemispherical dielectric resonator antenna (DRA) using low loss dielectric filament and high-conductive filaments jointly with a low-cost customized dual-extruding 3D printer. The parametric study consisted in the design and evaluation of five different hemispherical DRA topologies with different internal shapes and the same overall size, in which the printing infill percentage of the DRA was reduced. A 3D-printed metallic cap was included in the antenna to compensate for the resonant frequency shift in order to maintain its original dimensions. Measurement results show that all evaluated antennas kept the same resonant frequencies and similar radiation patterns while reducing the overall weight of the topology in 22% of the nominal weight.

INDEX TERMS 3D-printing, conductive filaments, dielectric resonator antennas, dielectric filaments.

I. INTRODUCTION

With 3D-printing technology, the possibility of manufacturing prototypes or functional parts incurring in a lower cost and reduced fabrication times has led to a new revolution on many applications [1]–[3]. In addition, the introduction of low-loss dielectric filaments [4] and high-conductive filaments [5] has enabled low-cost additive manufacturing of complex microwave topologies. In recent years, many studies has been focused on the high-frequency characterization of the materials used for 3D-printing [6]–[8] and on the fabrication of high-frequency structures such as metamaterials [9]–[11], antennas [12]–[15], dielectric lenses [16]–[20], amongst other implementations [21].

One particular structure that can directly benefit from the appearance of 3D-printing is that of dielectric resonator antennas (DRA). This well-known topology consists of a dielectric slab that can radiate depending on how it is excited. Its radiation characteristics and frequency depend on its dimensions, shape, and the relative permittivity of the dielectric slab, which makes it a versatile topology and that can have higher radiation efficiencies when compared to a standard microstrip implementation [22]. One of the main drawbacks of this technology is the limitation of available permittivity values on standard dielectric materials and that the complexity of the shape either increases the manufacturing cost or is limited by current manufacturing processes. This shape issue can be easily overcome by using 3D-printing, which allows the manufacture of different shapes, only depending on the precision of the printer, while for the permittivity values, we can obtain different dielectric constants just by varying the infill percentage of the 3D-printed dielectric [16], [17], [23].

Many studies have also been done on 3D-printed DRA, including wideband multi-ring structures [23], arrays [24], high-gain structures [25], and more original shape-synthesized DRA topologies [26]. One interesting option which has not been explored is combining in the same 3D-printing process the deposition of high-conductive and dielectric filaments to implement DRA topologies which uses both materials on the radiating structure (besides the feeding network and the ground plane). This kind of structure has been used in previous dielectric resonator antennas and filters, for example, to tune the resonant frequency of either the radiating or filtering mode of the resonator [27], [28]. Therefore, it is relevant to assess some insight about what 3D-printing achieves to give designers information referring to weight, cost, bandwidth, and cost of the overall structure.

Amongst the characteristics that can be controlled in the 3D-printing process of a DRA is the infill percentage of the

The associate editor coordinating the review of this manuscript and approving it for publication was Shah Nawaz Burokur.

material, which can affect either from an electromagnetic point of view or directly influence the overall weight of the structure [6], [29], [30]. In the specific case of 3D-printed dielectrics, reducing the infill percentage will reduce the relative permittivity of the structure [16], [17], shifting the resonance frequency of the antenna. To compensate for this effect, and as described in the previous paragraph, we can add a metallic cap and set the resonant frequency on any desired value [27]. Applying this principle, we can think of a 3D-printed DRA that can have a lower weight due to an infill percentage reduction and then using a conductive filament [5] to print a metallic cap on top of the dielectric section to compensate for the change in permittivity. Therefore, a weight reduction can be achievable and of interest for applications such as unmanned autonomous vehicles (UAVs), where the overall weight is an important parameter.

This article presents a parametric study related to the infill percentage of a fully 3D-printed hemispherical dielectric resonator antenna loaded with a metallic cap that operates at 5.8 GHz, which is a frequency used in vehicle-to-vehicle communications, and where we can find systems where weight relief can be an important feature for the radiating systems. The objective of the study is to assess the relation between infill-percentage and frequency tuning that can be achieved using the printed metallic cap on top of the hemispherical DRA, all by keeping the same volume and radiation characteristics of the original DRA, but reducing its overall weight. These characteristics are available for its implementation using a low cost 3D-printer, avoiding any precision machinery or milling for the dielectrics or the metallic cap. The article is divided into the following sections: in Section 2, the reference hemispherical DRA with a metallic cap operating at 5.8 GHz is presented. In Section 3, four different implementations of the same DRA varying the infill percentage are presented. In Section 4, the 3D-printing implementation of the antennas is introduced, while in Section 5, the measurement results are presented.

II. DIELECTRIC RESONATOR DESIGN AND SIMULATION

For this study, we will use as a reference case a hemispherical DRA loaded with a metallic cap based on the work published in [27]. This DRA is excited with a fundamental TE_{111} mode through an aperture coupling feeding, while the metallic cap is used to tune the resonant frequency of the antenna [27]. For our design, the antenna is sized to operate at 5.8 GHz, which corresponds to a frequency band used for vehicle-to-vehicle communication standards.

Figure 1 shows the proposed DRA. The relative permittivity used for the DRA is $\varepsilon_{DRA} = 10$, while the antenna is fed by an aperture coupled-feeding, etched on a FR-4 substrate of $\varepsilon_r = 4.4$, lateral dimensions of $L_{sub} = W_{sub} = 50$ mm, and height $h_{sub} = 1.7$ mm. Regarding the feeding network, a 50 Ω microstrip line of width $w_{line} = 3$ mm and length $L_{sub}/2 + l_{stub}$ (with $l_{stub} = 10$ mm), feeds an aperture etched on the ground plane of the substrate of dimensions $l_{slot} = 1.6$ mm and $w_{slot} = 8$ mm. This feeding network was

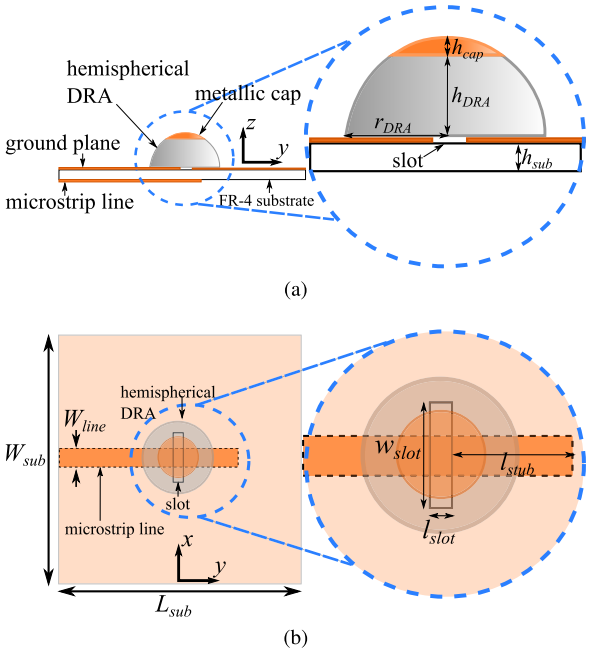

FIGURE 1. Reference hemispherical DRA with metallic cap. a) Side-view b) Top-view with aperture-feeding details.

decided to be designed using this standard substrate in order to avoid the losses introduced by the conductive filaments in this type of topologies in 3D-printing [6]. Finally, the antenna dimensions are a DRA radius of $r_{DRA} = 6$ mm and a height of $h_{DRA} = 5$ mm, while the metallic cap has a height of $h_{cap} = 1$ mm. It is worth noticing that without the metallic cap, that is to say, having a full dielectric hemispherical DRA of radius 6 mm, the resonance frequency of the antenna will be 6.2 GHz.

Figure 2 shows the simulated results of the reference DRA loaded with a metallic cap. Fig. 2a shows the reflection coefficients of the DRA, with and without the metallic cap, where the influence on the down-tuning of the frequency due to the metallic cap can be observed. The simulated gain radiation pattern of the DRA with metallic cap, calculated at 5.8 GHz, is depicted in Fig. 2b, where a maximum gain of around 5.7 dB can be seen for the antenna. In order to confirm the operating principle of the DRA, in Figure 3 is shown the simulated electric field on three different planes: x-y plane, y-z plane and x-z plane. We can see that the coupling slots feds the DRA with the previously described mode, to then radiates and generating the exposed radiation patterns. Having the reference antenna designed, now we proceed to design and set the DRA parameters to be assessed for this parametric study.

III. PARAMETRIC STUDY OF HEMISPHERICAL DRA LOADED WITH METALLIC CAP

We perform a parametric study with the designed reference DRA case, which is only possible due to the 3D-printing inherent characteristics. One parameter that can be important for antennas designed for vehicle communications, especially

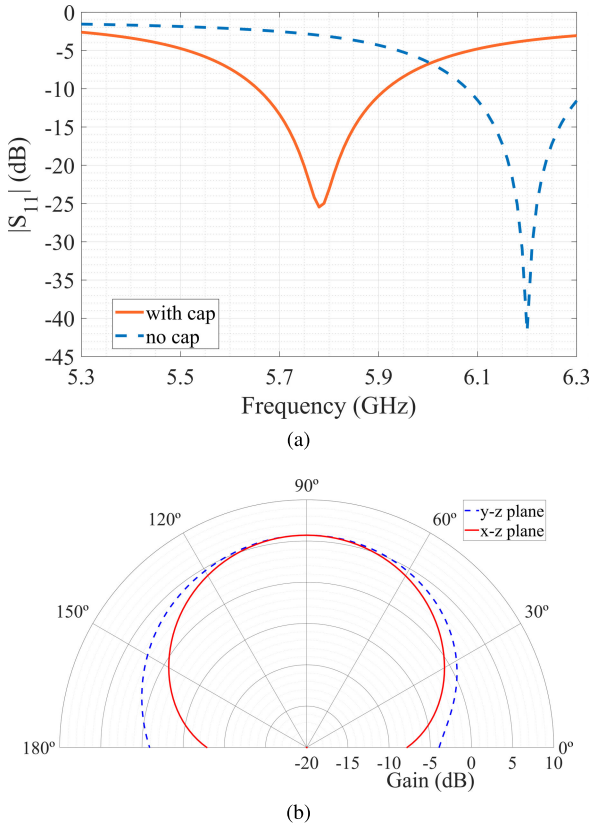

FIGURE 2. Simulated results of the reference DRA. a) $|S_{11}|$ as function of the frequency with and without the metallic cap (fully dielectric). b) Gain (in dB) for the y-z plane and x-z plane at 5.8 GHz with the metallic cap.

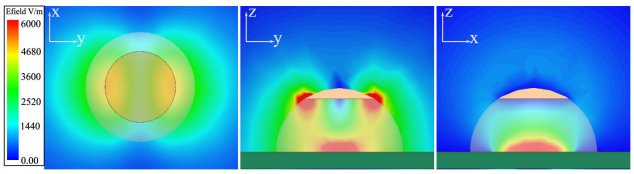

FIGURE 3. Simulated electric field at 5.8 GHz of the reference DRA on different planes. From left to right: x-y plane, y-z plane and x-z plane.

for unmanned autonomous vehicles (UAVs), is the weight of the antenna. In our case, the weight can be reduced by lowering the infill percentage of a portion of the 3D-printed dielectric resonator antenna, which will lower the relative permittivity of that section. This phenomenon will impact the resonant frequency of the DRA, which will be compensated by varying the height of the metal cap, keeping the original size of the DRA.

A. PROPOSED TOPOLOGIES FOR PARAMETRIC STUDY

For this study, two different topologies are analyzed, which are shown in Figure 4. The first topology (Fig. 4a) consists of the same hemispherical DRA previously analyzed, but the dielectric part is by divided into two horizontal layers with different infill percentages. In this topology, the section of the DRA named *DRA section 2* will have an infill percentage of 100%, while the section named *DRA section 1* will take two lower infill percentage values, i.e., 50% and 70%. The

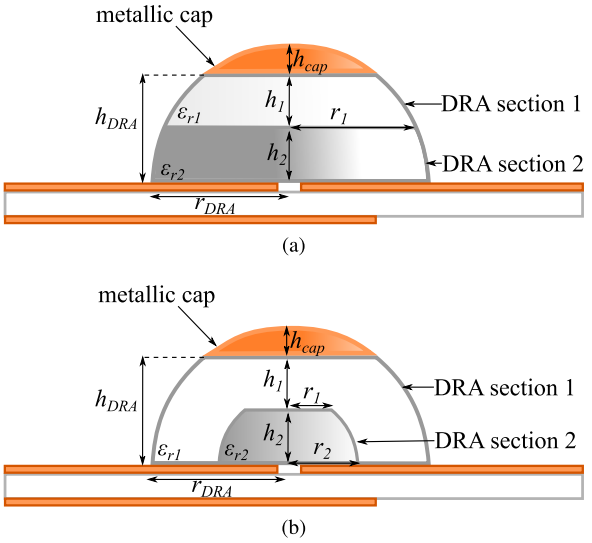

FIGURE 4. DRA antennas designed for the parametric study. a) Horizontally divided DRA with metallic cap. b) Dome-like divided DRA with metallic cap.

height of the metallic cap was increased so that the antenna operates at 5.8 GHz, compensating for the reduction of the permittivity values.

The second topology (Fig. 4b) is based on the same working principle as the previously proposed, i.e., one section will vary its infill percentage (*DRA section 1*) with the same declared infill percentages, i.e., 50% and 70%, while the other keeps a full infill (*DRA section 2*). The main difference is that besides the horizontal division, the full-infill section will have a reduced radius, giving the effect of a dome-like structure, where the lower infill percentage section contains the full-infill section of the DRA. As in the previous case, and due to the relative permittivity reduction, the metallic cap height is increased to have the antenna operating at 5.8 GHz.

A unit-cell analysis of the dielectric was conducted to obtain the relative permittivity value of the filament with the required infill percentage of this study. For this, a sub-lambda cubic unit-cell of dimensions $\lambda/6$ is filled with a dielectric with the relative permittivity of the filament in use. Two perfect conductor (PEC) plates placed on the top and bottom of the unit-cell to create a parallel plate condition and calculate its dispersion diagram. Then, by varying the infill percentage of the unit-cell, we retrieve the different dispersion diagrams, and therefore, the relative permittivity for each infill percentage variation. This unit-cell has proved to represent the infill percentage accurately and the relative permittivity obtained with the 3D-printing process [16], [17]. Figure 5 shows the unit-cell and the relative permittivity values as a function of the infill percentage obtained with this analysis for the filament PREPERM ABS1000 ($\varepsilon_r = 10$).

From Figure 5 we can retrieve the relative permittivity when using 70% and 50% infill percentages, corresponding to a relative permittivity values of $\varepsilon_r = 6.6$ and $\varepsilon_r = 4.78$, respectively, using the fitted curve obtained with MatLab by

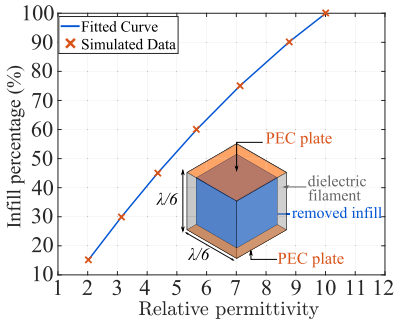

FIGURE 5. Relative permittivity values of the ABS1000 filament as function of the infill percentage and the corresponding sub-lambda unit-cell used for its calculation.

TABLE 1. Simulated hemispherical DRA and its dimensions for its operation at 5.8 GHz.

DRA type	infill	dimensions (mm)				
		h_1	h_2	h_{cap}	r_1	r_2
horizontal divided	70%	2.10	2.10	1.8	4.28	-
	50%	1.60	1.60	2.80	5.07	
dome-like	70%	1.85	1.85	2.30	3.08	3.60
	50%	1.10	1.10	3.80	3.42	3.60

the following equation (where x is the relative permittivity):

$$ABS1000(\varepsilon_r) = -0.003893x^2 + 0.1531x - 0.1425 \quad (1)$$

These values are the ones that will be used for the different DRA implementations on the variations of *DRA Section 1*.

B. SIMULATION RESULTS

Once we defined the permittivity values corresponding to both infill percentages that will vary in the *DRA Section 1* of both implementations, we proceeded to simulate the four different implementations of the hemispherical DRA with the metallic cap using ANSYS HFSS [31]. That is to say, two implementations of the horizontally divided model (Fig. 4a) using the two permittivity values obtained with the infill percentages, i.e., 50% and 70% infill, and two implementations using the same permittivity variations for the dome-like topology (Fig. 4b). For these antennas, the scope is to keep the resonant frequency of the DRA at 5.8 GHz, by compensating the reduction of permittivity values by using the metallic cap to keep the same volume of the original hemispherical DRA presented in Figure 1, i.e., $h_{DRA} + h_{cap} = r_{DRA} = 6$ mm. Table 1 presents the corresponding dimension of each DRA under study that assures an operational frequency of 5.8 GHz. For these simulations, the metallic cap and the dielectrics used in the DRA are considered lossless.

Figure 6 and Figure 7 show the simulated reflection coefficient $|S_{11}|$ as a function of the frequency and the gain radiation pattern (in dB) for the horizontally divided DRA and for the dome-like divided DRA, respectively. These values are compared with the reference case previously exposed (100% infill). We can see that in all the implementations, the antenna is well matched at 5.8 GHz, which confirms that we can compensate for the effect of reducing the infill percentage (and therefore the relative permittivity of the section) by modifying

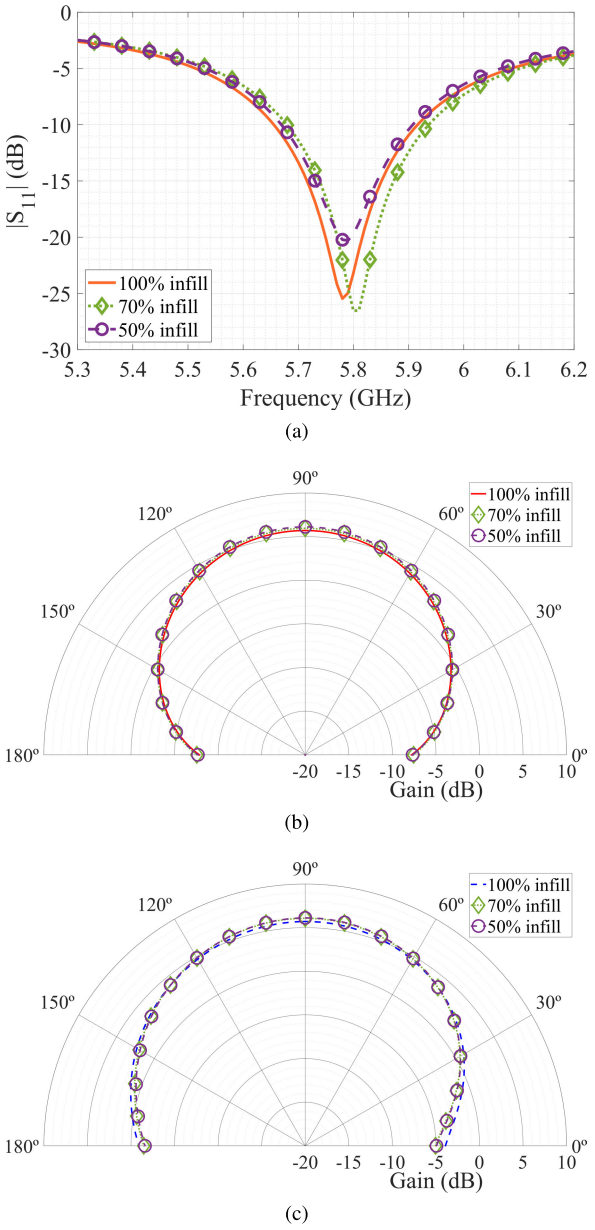

FIGURE 6. Simulated results of the horizontal parametric study as a function of different infill percentages for DRA section 1. a) $|S_{11}|$ as a function of the frequency. b) Gain (in dB) for the x-z plane at 5.8 GHz. c) Gain (in dB) y-z plane at 5.8 GHz.

the height of the metallic cap. Regarding the obtained gain radiation patterns, we can see no significant variation of the radiation on both planes for the four different antennas when compared to the reference case.

The obtained simulation results confirm that we can reduce the infill percentage of a section of the resonator of a hemispherical DRA operating at 5.8 GHz, while keeping the same radiation characteristics and volume of a full-infill (full-weight) implementation by compensating the infill reduction with a metallic cap.

One important parameter that has to be taken into account is the finite conductivity of the conductive filament that will

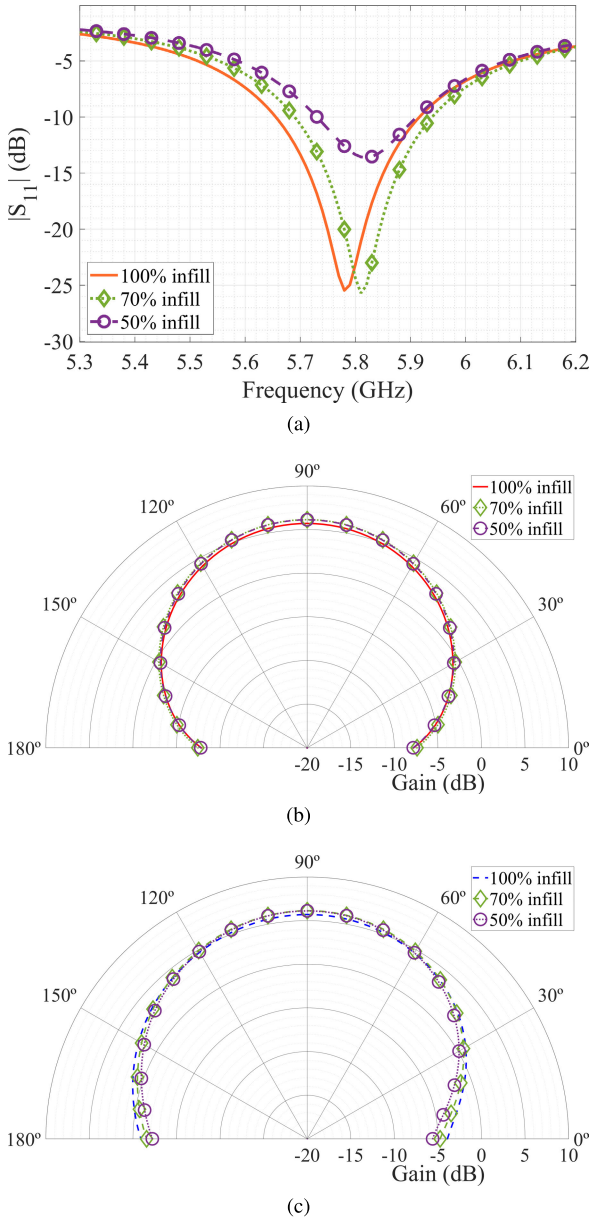

FIGURE 7. Simulated results of the dome-like parametric study as a function of different infill percentages for DRA section 1. a) $|S_{11}|$ as a function of the frequency. b) Gain (in dB) for the x-z plane at 5.8 GHz. c) Gain (in dB) y-z plane at 5.8 GHz.

be used for the metallic cap. Previous studies on this filament confirms that at higher frequencies the losses introduced by the filament tends to increase [6], [8]. On the other hand, we need to take into account the losses that can be additionally introduced by the ABS filament used in the DRA. For the following simulation results we used the declared value of dielectric losses for the PREPERM ABS1000 filament of $\tan\,\delta\,=\,0.003$ [4]. For the conductive filament, we will use two values for simulation. First, the declared value of 1.6×10^4 S/m declared by the manufacturer [5], and a second simulation using a reduced conductivity value of 1000 S/m, which can be estimated from previous measured results at the operating frequency [6], [9]. To notice that this value is just

TABLE 2. Ocular3D EIE-custom 3D printer technical specifications.

Printer parameter	Value
Maximum printing volume	$190\times190\times190$ mm^3
Axis resolution	100 μm in all axis *(xyz)*
Hot-end model	Two E3DV6 [33]
Hot-end T° range	120 to 280°C
Platform maximum T°	100°C

an estimation for the conductivity value based on a retrofitted simulation to obtain a similar loss effect obtained in measurement of the previous works at the resonance frequency of the DRA. In Figure 8 are exposed the simulated realized gains (in dB) at 5.8 GHz for the two different implementations of the parametric study, as function of the infill and the different conductivity values used for the metallic cap.

We can see from the simulation results that when the conductivity value is assumed with $\sigma\,=\,1.6\,\times\,10^4$ S/m, the realized gain is not significantly affected if compared to the case when using a perfect conductor. However, when the conductivity value is assumed with $\sigma\,=\,1000$ S/m, we can see a significant reduction of the maximum gain in all the implementations, being more important when the metallic cap is larger, that is to say, when the infill percentage of the dielectric section is lower. In brief, the maximum gain for this low conductivity value goes from 3.7 dB to 4.4 dB. With this simulation assessment, we can proceed to design and manufacture the five DRA under study to be suitable for a 3D-printing process.

IV. 3D-PRINTING ANTENNA DESIGN

To manufacture the different antennas under study, we use a custom-ordered 3D-printer from Ocular3D [32]. This double-extruder 3D-printer has the technical characteristics in terms of hot-ends and bed temperature that allow it to print the Electrifi conductive filament and the ABS dielectric filament provided by PREPERM [9], [17] jointly. The 3D-printer in use is shown in Figure 9, while Table 2 summarizes its main technical specifications.

The software Ultimaker Cura [34] was used to generate the gcode for the 3D-printer, which permits the user to specify different parameters for the 3D-printing process: the bed and extruding temperatures, extruding speed, infill percentage, and infill patterns, amongst other relevant parameters that are important for a correct deposition of the filaments. Figure 10 depicts two cut-views in Ultimaker Cura of the 70% infill hemispherical DRA, where we can see the metallic cap and both dielectric sections of the DRA with the different infill percentages, i.e., 100% for *DRA section 2* and 70% for *DRA section 1*.

Table 3 presents the main printing parameters used for the deposition of both dielectric (ABS1000) and conductive filament, and Figure 11 shows the five manufactured 3D-printed hemispherical DRA for the study. It is worth noticing that the substrate in use for the feeding network is a FR-4 substrate ($\varepsilon_r\,=\,4.4$) with a height of $h_{sub}\,=\,1.6$ mm and lateral dimensions of 50 mm$\times$50 mm, and a 50 Ω SMA connector is soldered to the microstrip line for measurements.

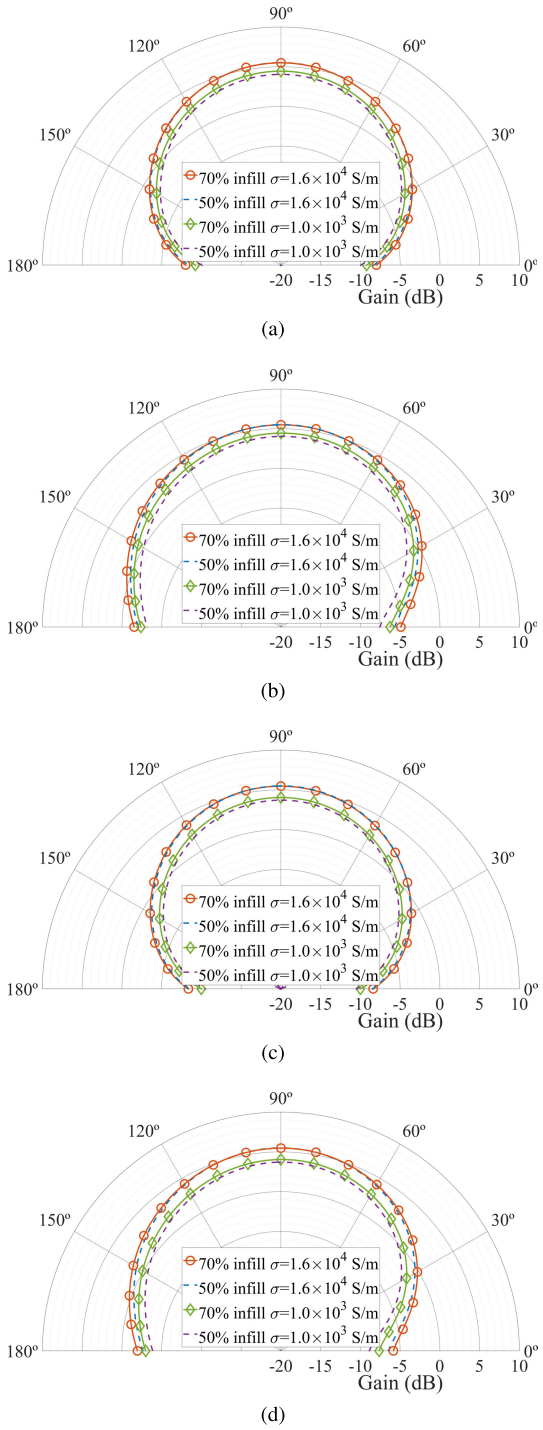

FIGURE 8. Realized gain at 5.8 GHz for two different DRA implementations, as function of the infill percentage and conductivity of the metallic cap. a) Horizontally divided x-z plane. b) Horizontally divided y-z plane. c) Dome-like x-z plane. d) Dome-like y-z plane.

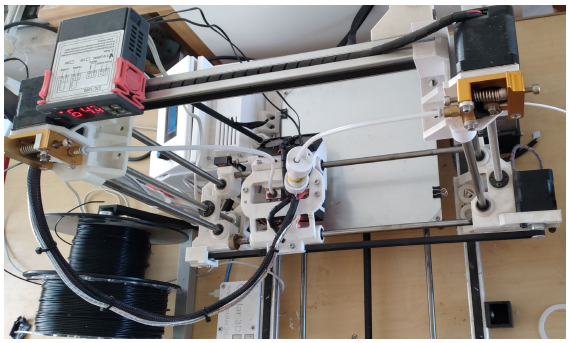

FIGURE 9. Custom 3D-printer manufactured by Ocular3D.

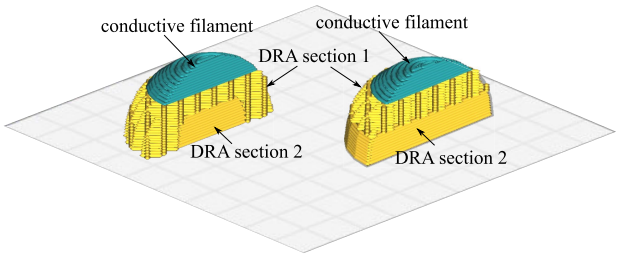

FIGURE 10. Cut-view of the 3D-printed DRA with the different sections generated with Ultimaker Cura.

TABLE 3. 3D-printing parameter for the filaments used for the antenna construction.

3D-printing parameter	Conductive filament	ABS1000 filament
Printing temp. (C°)	160	250
Printing speed (mm/s)	15	15
Flow (%)	120	100
Retraction distance (mm)	-	3.5
Printing pattern	automatic	automatic
Build plate temp. (C°)	80	80

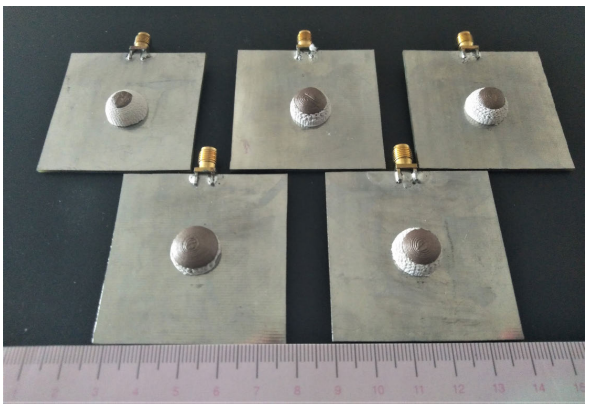

FIGURE 11. 3D-printed antennas with their corresponding feeding network.

V. MEASUREMENT RESULTS

Once the devices were constructed, we proceeded to measure the reflection coefficient as a function of the frequency and the gain radiation pattern in both planes of the DRA. The first measurements of the reflection coefficient showed a similar frequency shift in their resonance frequencies. This can be attributed to a slightly different value of the relative permittivity of the dielectric filament and the uncertainty of the relative permittivity that exhibits the conductive filament. We resized the antennas to compensate for this frequency shift, including resizing the metallic cap section within the range of resolution of the 3D-printer. Table 4 shows the new dimensions of the antennas.

TABLE 4. Dimensions of the 3D-printed constructed antennas.

DRA type	infill	dimensions (mm)				
		h_1	h_2	h_{cap}	r_1	r_2
horizontal divided	70%	2.5	2.5	1.8	6.3	-
	50%	2.0	2.0	2.8	6.5	
dome-like	70%	2.2	2.2	2.4	3.4	4.1
	50%	1.5	1.5	3.8	3.8	4.1

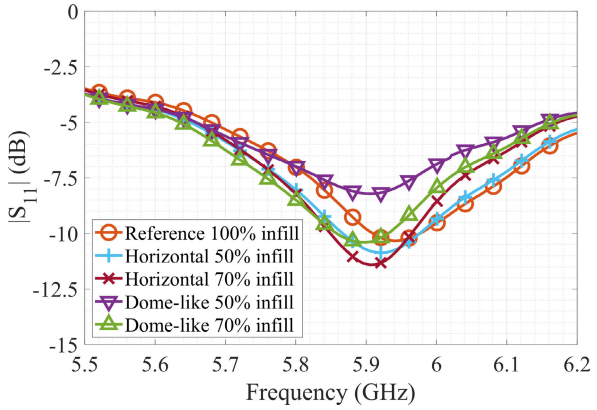

FIGURE 12. Measured $|S_{11}|$ parameter as function of the frequency for the constructed antennas.

In Figure 12 are shown the measured reflection coefficient $|S_{11}|$. We can see that the resonant frequencies of the antennas are around $f_0 = 5.9$ GHz in all implementations. The resonance frequency difference can be explained due to slight differences in the dielectric filament relative permittivity and the permittivity introduced by the conductive filament, and the fabrication tolerance of a multisection structure. In addition, we can see that most of the implementations are matched at f_0, except for the one named *Dome-like 50% infill*. This mismatching can be explained due to the difference of the relative permittivity value of the filament, which is a parameter that can affect the dimensions of the slot to obtain the desired coupling [35], and in this case and due to the geometric distribution of the dome-like DRA, is the more sensitive topology to this kind of variations at the slot level.

All five implementations were measured in an anechoic chamber to obtain their gain radiation patterns at their resonance frequencies f_0, for the same planes obtained in the simulation. Figure 13 shows the gain radiation patterns at f_0 for the five 3D-printed antennas on the x-z plane and the y-z plane. From the measurement results, we can observe that the maximum overall gain in the simulation is higher than the obtained in measurements, varying from 3.8 dBi to 4.7 dBi, which is in line with the previous simulation results previously exposed, when using a low conductivity value for the metallic cap. Therefore, this difference can be explained mainly due to the losses inserted by the dielectric filament and the losses introduced by the conductive filament. However, there are studies that demonstrates that this particular filament is suitable for electrodeposition, which can increase the conductivity of the filament with a simple chemical process, and by consequence, compensate these losses [7]. In addition, this implementation, as-is, exhibits better performance in

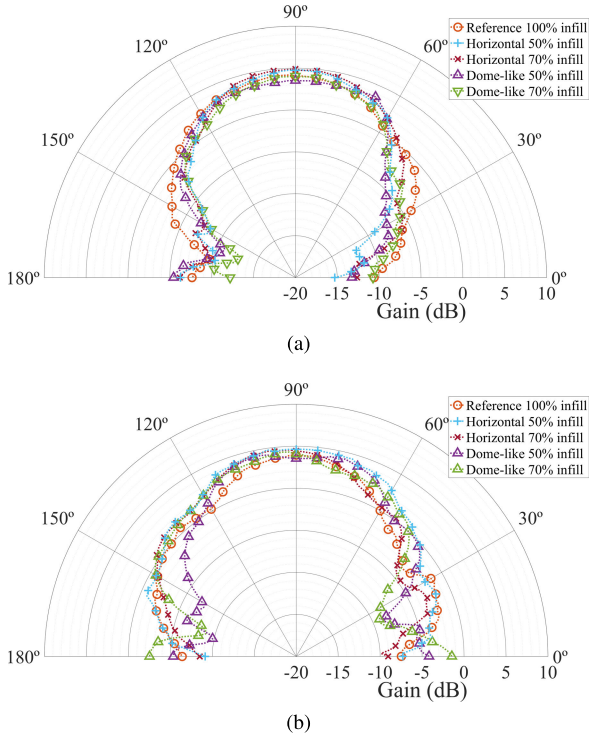

FIGURE 13. Measured gain radiation patterns (in dB) for the different 3D-printed antennas at f_0. a) x-z plane. b) y-z plane.

terms of realized gain when compared to a fully 3D-printed patch antenna using the same conductive filament [6]. Finally, and regarding the shape of the obtained patterns, we can see that the implementations have a similar radiation pattern in both planes, except for the dome-like implementations, which have more considerable differences at lower angles.

TABLE 5. Weight estimation in milligrams for each 3D-printed antenna.

3D-printed antenna	Antenna section	Material used	Infill %	Material estimation	
				mg	Total (mg)
Reference DRA	Cap (1 mm)	Electrifi	100%	23	**727**
	DRA	ABS1000	100%	704	
Horizontal 50% infill	Cap (2.8 mm)	Electrifi	100%	171	**610**
	DRA Section 1	ABS1000	50%	128	
	DRA Section 2	ABS1000	100%	311	
Horizontal 70% infill	Cap (1.8 mm)	Electrifi	100%	73	**597**
	DRA Section 1	ABS1000	70%	178	
	DRA Section 2	ABS1000	100%	346	
Dome-like 50% infill	Cap (3.8 mm)	Electrifi	100%	300	**568**
	DRA Section 1	ABS1000	50%	186	
	DRA Section 2	ABS1000	100%	83	
Dome-like 70% infill	Cap (2.4 mm)	Electrifi	100%	129	**577**
	DRA Section 1	ABS1000	70%	333	
	DRA Section 2	ABS1000	100%	115	

Another point to discuss is the weight reduction obtained on each implementation. Table 5 summarizes the used material on each implementation, in milligrams, for each section of the antenna and total. From the table, we can see that by reducing the infill percentage and compensating the size of the metallic cap, we can obtain lighter antennas with

similar behavior in terms of resonance frequency and radiation pattern. A maximum reduction of 159 mg is obtained compared to the reference case, which corresponds to a reduction of around 22% of the nominal weight of the antenna. This weight reduction can be more important if we consider the use of standard dielectrics for the construction of the DRA. For example, if we use alumina ($\varepsilon_r \approx 10$) [36], [37], for the fabrication of this same DRA and giving the mass density of alumina of around 3.95 g/cm^3, an estimated weight of the DRA can take values of 2600 mg, which is around 4.5 times higher than the lighter proposed structure in this work. This result can be important for example when designing an antennae system for UAVs, or any other system where size and weight is an important issue, moreover if it is used for on-board antenna arrays, where we have an increment of the radiating elements.

Finally, we can compare this implementation with other 3D-printed DRA topologies and more innovative DRA topologies operating in the same frequency band [29], [38]. The results obtained in terms of realized gains in the same frequency are within a comparable range values with other implementations, but this proposed work can offer a reduced size and wight reduction due to the infill percentages, that can implies a also having a reduced weight when compared to other implementations [29], [38]–[42].

VI. CONCLUSION

This article presented a parametric study concerning the infill percentage and internal shape of a fully 3D-printed hemispherical dielectric resonator antenna with a metallic cap to reduce its nominal resonance frequency. The obtained results show that it is possible to compensate for reducing the infill percentage, which changes the resonance frequency of the different DRA implementations, by using a 3D-printed metallic cap and varying its dimensions. Measurement results show that all 3D-printed implementations operate in a similar resonant frequency and have similar radiation patterns, except for minor differences. These differences can be explained due to width variations of the printed filament or additional reflections associate with the infill pattern when infill percentage is low. Finally, and regarding the weight reduction obtained with this technique, a maximum of 22% of weight reduction was achieved compared to a reference case that uses a 100% infill percentage for the filaments. This weight reduction and the overall size of the implemented DRAs can be interesting when implementing this antenna topology in antenna arrays for applications such as unmanned aerial vehicles (UAV), or any other system where size and weight are critical parameters to be considered in the design. For example, if we consider the implementation of an antenna array at this same frequency using patch antennas, each individual element will be larger in size (around 33% larger for each element using the same substrate for the feeding network of the DRA) which can critical depending on the available space of the system.

ACKNOWLEDGMENT

The authors would like to thank PREPERM for its support for the dielectric filaments and Universidad Técnica Federico Santa María, Chile, for the measurements in anechoic chamber.

REFERENCES

[1] E. Macdonald, R. Salas, D. Espalin, M. Perez, E. Aguilera, D. Muse, and R. B. Wicker, "3D printing for the rapid prototyping of structural electronics," *IEEE Access*, vol. 2, pp. 234–242, Dec. 2014.

[2] C. Kim, D. Espalin, M. Liang, H. Xin, A. Cuaron, I. Varela, E. Macdonald, and R. B. Wicker, "3D printed electronics with high performance, multilayered electrical interconnect," *IEEE Access*, vol. 5, pp. 25286–25294, 2017.

[3] S. Willis, "The maker revolution," *Computer*, vol. 51, no. 3, pp. 62–65, Mar. 2018.

[4] *Premix Preperm Website*. Accessed: Mar. 3, 2021. [Online]. Available: https://www.preperm.com

[5] *Multi3D Website*. Accessed: Mar. 3, 2021. [Online]. Available: https://www.multi3dllc.com/

[6] F. Pizarro, R. Salazar, E. Rajo-Iglesias, M. Rodriguez, S. Fingerhuth, and G. Hermosilla, "Parametric study of 3D additive printing parameters using conductive filaments on microwave topologies," *IEEE Access*, vol. 7, pp. 106814–106823, 2019.

[7] M. J. Kim, M. A. Cruz, S. Ye, A. L. Gray, G. L. Smith, N. Lazarus, C. J. Walker, H. H. Sigmarsson, and B. J. Wiley, "One-step electrodeposition of copper on conductive 3D printed objects," *Additive Manuf.*, vol. 27, pp. 318–326, May 2019.

[8] S. Roy, M. B. Qureshi, S. Asif, and B. D. Braaten, "A model for 3D-printed microstrip transmission lines using conductive electrifi filament," in *Proc. IEEE Int. Symp. Antennas Propag., USNC/URSI Nat. Radio Sci. Meeting*, Jul. 2017, pp. 1099–1100.

[9] P. Stuardo, F. Pizarro, and E. Rajo-Iglesias, "3D-printed sievenpiper metasurface using conductive filaments," *Materials*, vol. 13, no. 11, p. 2614, Jun. 2020.

[10] A. C. Tasolamprou, D. Mentzaki, Z. Viskadourakis, E. N. Economou, M. Kafesaki, and G. Kenanakis, "Flexible 3D printed conductive metamaterial units for electromagnetic applications in microwaves," *Materials*, vol. 13, no. 17, p. 3879, Sep. 2020.

[11] Y. Xie, S. Ye, C. Reyes, P. Sithikong, B.-I. Popa, B. J. Wiley, and S. A. Cummer, "Microwave metamaterials made by fused deposition 3D printing of a highly conductive copper-based filament," *Appl. Phys. Lett.*, vol. 110, no. 18, May 2017, Art. no. 181903.

[12] Y. Li, L. Ge, J. Wang, S. Da, D. Cao, J. Wang, and Y. Liu, "3-D printed high-gain wideband waveguide fed horn antenna arrays for millimeter-wave applications," *IEEE Trans. Antennas Propag.*, vol. 67, no. 5, pp. 2868–2877, May 2019.

[13] S. Moscato, R. Bahr, T. Le, M. Pasian, M. Bozzi, L. Perregrini, and M. M. Tentzeris, "Infill-dependent 3-D-printed material based on NinjaFlex filament for antenna applications," *IEEE Antennas Wireless Propag. Lett.*, vol. 15, pp. 1506–1509, 2016.

[14] Y. Li, C. Wang, H. Yuan, N. Liu, H. Zhao, and X. Li, "A 5G MIMO antenna manufactured by 3-D printing method," *IEEE Antennas Wireless Propag. Lett.*, vol. 16, pp. 657–660, 2017.

[15] Y. Tawk, M. Chahoud, M. Fadous, J. Costantine, and C. G. Christodoulou, "The miniaturization of a partially 3-D printed quadrifilar helix antenna," *IEEE Trans. Antennas Propag.*, vol. 65, no. 10, pp. 5043–5051, Oct. 2017.

[16] O. Bjorkqvist, O. Zetterstrom, and O. Quevedo-Teruel, "Additive manufactured dielectric gutman lens," *Electron. Lett.*, vol. 55, no. 25, pp. 1318–1320, Dec. 2019.

[17] J.-M. Poyanco, F. Pizarro, and E. Rajo-Iglesias, "3D-printing for transformation optics in electromagnetic high-frequency lens applications," *Materials*, vol. 13, no. 12, p. 2700, Jun. 2020.

[18] A. Belen, F. Güneş, P. Mahouti, and M. Palandöken, "A novel design of high performance multilayered cylindrical dielectric lens antenna using 3D printing technology," *Int. J. RF Microw. Comput.-Aided Eng.*, vol. 30, no. 1, p. e21988, Jan. 2020.

[19] M. A. Belen and P. Mahouti, "Design of nonuniform substrate dielectric lens antennas using 3D printing technology," *Microw. Opt. Technol. Lett.*, vol. 62, no. 2, pp. 756–762, Feb. 2020.

[20] P. Mahouti, M. A. Belen, F. Güneş, and R. Yurt, "Design and realization of multilayered cylindrical dielectric lens antenna using 3D printing technology," *Microw. Opt. Technol. Lett.*, vol. 61, no. 5, pp. 1400–1403, May 2019.
[21] S.-H. Shin, X. Shang, N. M. Ridler, and S. Lucyszyn, "Polymer-based 3-D printed 140–220 GHz low-cost quasi-optical components and integrated subsystem assembly," *IEEE Access*, vol. 9, pp. 28020–28038, 2021.
[22] Q. Lai, G. Almpanis, C. Fumeaux, H. Benedickter, and R. Vahldieck, "Comparison of the radiation efficiency for the dielectric resonator antenna and the microstrip antenna at Ka band," *IEEE Trans. Antennas Propag.*, vol. 56, no. 11, pp. 3589–3592, Nov. 2008.
[23] Z.-X. Xia, K. W. Leung, and K. Lu, "3-D-printed wideband multi-ring dielectric resonator antenna," *IEEE Antennas Wireless Propag. Lett.*, vol. 18, no. 10, pp. 2110–2114, Oct. 2019.
[24] A. A. Althuwayb, K. A. Abdalmalak, C. S. Lee, G. Santamaría-Botello, L. E. García-Castillo, D. Segovia-Vargas, and L. E. García-Muñoz, "3-D-printed dielectric resonator antenna arrays based on standing-wave feeding approach," *IEEE Antennas Wireless Propag. Lett.*, vol. 18, no. 10, pp. 2180–2183, Oct. 2019.
[25] E. Baldazzi, A. Al-Rawi, R. Cicchetti, A. B. Smolders, O. Testa, C. D. J. V. C. Moreno, and D. Caratelli, "A high-gain dielectric resonator antenna with plastic-based conical horn for millimeter-wave applications," *IEEE Antennas Wireless Propag. Lett.*, vol. 19, no. 6, pp. 949–953, Jun. 2020.
[26] H. Alroughani and D. A. McNamara, "The shape synthesis of dielectric resonator antennas," *IEEE Trans. Antennas Propag.*, vol. 68, no. 8, pp. 5766–5777, Aug. 2020.
[27] H. K. Ng and K. W. Leung, "Frequency tuning of the dielectric resonator antenna using a loading cap," *IEEE Trans. Antennas Propag.*, vol. 53, no. 3, pp. 1229–1232, Mar. 2005.
[28] L. K. Hady, D. Kajfez, and A. A. Kishk, "Triple mode use of a single dielectric resonator," *IEEE Trans. Antennas Propag.*, vol. 57, no. 5, pp. 1328–1335, May 2009.
[29] Z.-X. Xia and K. W. Leung, "3D-printed wideband rectangular dielectric resonator antenna," in *Proc. Photon. Electromagn. Res. Symp.-Fall (PIERS-Fall)*, Dec. 2019, pp. 285–289.
[30] J. Huang, S. J. Chen, Z. Xue, W. Withayachumnankul, and C. Fumeaux, "Impact of infill pattern on 3D printed dielectric resonator antennas," in *Proc. IEEE Asia–Pacific Conf. Antennas Propag. (APCAP)*, Aug. 2018, pp. 233–235.
[31] *ANSYS Website*. Accessed: Mar. 3, 2021. [Online]. Available: https://www.ansys.com/
[32] *Ocular 3D Website*. Accessed: Mar. 3, 2021. [Online]. Available: http://ocular3d.cl/
[33] *E3D Website*. Accessed: Mar. 3, 2021. [Online]. Available: https://e3d-online.com
[34] *Ultimaker Cura Website*. Accessed: Mar. 3, 2021. [Online]. Available: https://ultimaker.com/
[35] K. W. Leung, K. M. Luk, and D. Lin, "Input impedance of aperture coupled hemispherical dielectric resonator antenna," *Electron. Lett.*, vol. 29, no. 13, pp. 1165–1167, Jun. 1993.
[36] B. Sahu, P. Tripathi, S. Singh, M. K. Meshram, and S. P. Singh, "A simple structured filtering dielectric resonator antenna," in *Proc. IEEE Uttar Pradesh Sect. Int. Conf. Electr., Comput. Electron. Eng. (UPCON)*, 2016, pp. 543–545.
[37] U. Dey and J. Hesselbarth, "Spherical dielectric resonator antenna operating at 180 GHz," *IEEE Antennas Wireless Propag. Lett.*, vol. 19, no. 8, pp. 1380–1384, Aug. 2020.
[38] S. Maity and B. Gupta, "Experimental investigations on wideband triangular dielectric resonator antenna," *IEEE Trans. Antennas Propag.*, vol. 64, no. 12, pp. 5483–5486, Dec. 2016.
[39] C. Yang, Y. Xiao, and K. W. Leung, "A 3D-printed wideband multilayered cylindrical dielectric resonator antenna with air layers," in *Proc. IEEE Asia–Pacific Microw. Conf. (APMC)*, Dec. 2020, pp. 561–563.
[40] M. Khalily, M. R. Kamarudin, M. Mokayef, and M. H. Jamaluddin, "Omnidirectional circularly polarized dielectric resonator antenna for 5.2-GHz WLAN applications," *IEEE Antennas Wireless Propag. Lett.*, vol. 13, pp. 443–446, 2014.
[41] X. S. Fang, L. P. Weng, and Y.-X. Sun, "Slots-coupled omnidirectional circularly polarized cylindrical glass dielectric resonator antenna for 5.8-GHz WLAN application," *IEEE Access*, vol. 8, pp. 204718–204727, 2020.
[42] A. Iqbal, A. J. Alazemi, and N. K. Mallat, "Slot-DRA-based independent dual-band hybrid antenna for wearable biomedical devices," *IEEE Access*, vol. 7, pp. 184029–184037, 2019.

MATIAS CUEVAS was born in Rancagua, Chile, in 1994. He received the degree in ingeniero civil electrónico from the Pontificia Universidad Católica de Valparaíso (PUCV), Chile, in 2019. He has been a Research Assistant with PUCV, collaborating on topics related to RF location for mobile robots on and 3D-printed high frequency devices using conductive filaments.

FRANCISCO PIZARRO (Member, IEEE) received the degree in electronic engineering from the Pontificia Universidad Católica de Valparaíso, Chile, in 2010, the M.Sc. degree in communication engineering from the Politecnico di Torino, Italy, in 2010, and the Ph.D. degree in electromagnetics and high frequency systems, plasma engineering from the Institut Supérieur de l'Aéronautique et de l'Espace, Toulouse, France, in 2014. Since 2014, he has been an Associate Professor with the School of Electrical Engineering, Pontificia Universidad Católica de Valparaíso. His research interests include 3D-printed antennas, metamaterials, and plasma/microwave interaction.

ARIEL LEIVA received the B.Sc. degree in electronic engineering and the M.Sc. degree in electrical engineering from the Pontificia Universidad Católica de Valparaíso (PUCV), Chile, in 2003 and 2007, respectively, and the Ph.D. degree from Universidad Técnica Federico Santa María, Valparaiso, Chile, in 2013. He is currently a Lecturer with PUCV. His current interests include fiber optic communication systems and optical networking.

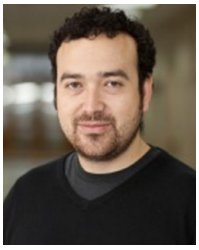

GABRIEL HERMOSILLA received the degree in electronic engineering from the University of La Frontera, Temuco, Chile, in 2007, and the Ph.D. degree in electrical engineering from the University of Chile, Santiago, Chile, in 2012. He is currently an Associate Professor with the School of Electrical Engineering, Pontificia Universidad Católica de Valparaíso (PUCV), Valparaiso, Chile. His research interests include thermal face recognition, pattern recognition, deep learning, and computer vision.

DANIEL YUNGE (Member, IEEE) was born in Valdivia, Chile, in 1984. He received the degree in electronics engineering from the Pontifical Catholic University of Valparaiso (PUCV), Chile, in 2009, and the Ph.D. degree from the Technical University of Munich (TUM), Germany, in 2019. He is currently an Associate Professor with the School of Electrical Engineering, PUCV. His research interests include low-power design techniques for the wireless IoT devices and mixed-signal and DSP design techniques for sensing devices.